BIOCHEMISTRY
including biophysical chemistry & molecular biology

ARTICLE

pubs.acs.org/biochemistry

Mechanistic Studies of Reactions of Peroxodiiron(III) Intermediates in T201 Variants of Toluene/*o*-Xylene Monooxygenase Hydroxylase

Woon Ju Song and Stephen J. Lippard*

Department of Chemistry, Massachusetts Institute of Technology, Cambridge, Massachusetts 02139, United States

Supporting Information

ABSTRACT: Site-directed mutagenesis studies of a strictly conserved T201 residue in the active site of toluene/*o*-xylene monooxygenase hydroxylase (ToMOH) revealed that a single mutation can facilitate kinetic isolation of two distinctive peroxodiiron(III) species, designated $T201_{peroxo}$ and $ToMOH_{peroxo}$, during dioxygen activation. Previously, we characterized both oxygenated intermediates by UV−vis and Mössbauer spectroscopy, proposed structures from DFT and QM/MM computational studies, and elucidated chemical steps involved in dioxygen activation through the kinetic studies of $T201_{peroxo}$ formation. In this study, we investigate the kinetics of $T201_{peroxo}$ decay to explore the reaction mechanism of the oxygenated intermediates following O_2 activation. The decay rates of $T201_{peroxo}$ were monitored in the absence and presence of external (phenol) or internal (tryptophan residue in an I100W variant) substrates under pre-steady-state conditions. Three possible reaction models for the formation and decay of $T201_{peroxo}$ were evaluated, and the results demonstrate that this species is on the pathway of arene oxidation and appears to be in equilibrium with $ToMOH_{peroxo}$.

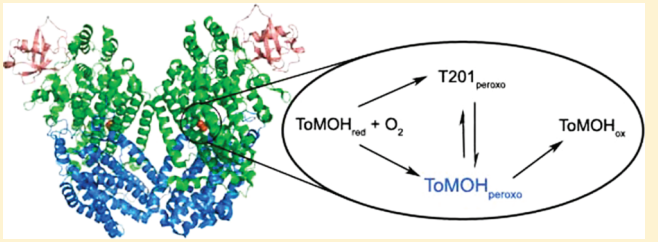

Bacterial multicomponent monooxygenases (BMMs) are capable of activating dioxygen and catalyzing selective organic substrate oxidation.[1,2] The BMMs contain carboxylate-bridged nonheme diiron centers, now a common motif in metalloenzymes,[3] including ribonucleotide reductases,[4] desaturases,[5] *myo*-inositol oxygenase,[6] human deoxyhypusine hydroxylase,[7] amine oxygenase,[8] and a recently characterized enzyme on the ubiquinone biosynthesis pathway.[9] Studies of BMMs have mainly focused on soluble methane monooxygenase hydroxylase (sMMOH), revealing two peroxodiiron(III) (P* and P or H_{peroxo}) and a diiron(IV) species (Q) that are generated during dioxygen activation in the presence of a regulatory protein (MMOB).[10−15] Recently, we have been investigating the toluene/*o*-xylene monooxygenase hydroxylase (ToMOH) component of toluene/*o*-xylene monooxygenase (ToMO), which evolved from an ancestor similar to that of sMMO.[16,17] Because the two hydroxylases share very similar diiron active site structures,[18] it seemed plausible that their dioxygen activation mechanisms might proceed through analogous peroxodiiron(III)- and Q-type intermediates. Pre-steady-state studies of dioxygen activation by reduced ToMOH in the presence of its cognate regulatory protein ToMOD (hereafter $ToMOH_{red}D$), however, revealed that this enzyme system generates a previously unprecedented diiron(III) intermediate, $ToMOH_{peroxo}$ (Chart 1A).[19] Moreover, no evidence of formation of a Q-like species has yet been found in ToMOH reactions. These results imply that ToMOH has an O_2 activation profile different from that of sMMOH, oxidizing its substrates via different intermediates.

Pre-steady-state studies of dioxygen activation in ToMOH are hampered by the absence of an optical band in the $ToMOH_{peroxo}$ intermediate. By perturbing the active site structure through the generation of Ser, Cys, and Gly variants of ToMOH T201, however, a residue strictly conserved and located close to the diiron centers in all BMMs, we discovered a novel intermediate, $T201_{peroxo}$. This species forms in addition to $ToMOH_{peroxo}$ in these variants.[20,21] $T201_{peroxo}$ exhibits UV−vis and Mössbauer spectra similar to those of H_{peroxo} in sMMOH (Chart 1B), and its optical feature allowed us to obtain kinetic parameters of its formation by stopped-flow spectroscopy in the T201 variants under a variety of reaction conditions. Rates of formation of $T201_{peroxo}$ in the T201S variant are proportional to the concentration of O_2, a result that allowed us to determine the likely pathway by which dioxygen accesses the active site diiron center.[22] DFT and QM/MM calculations revealed how the conformation of the side chain at T201 site perturbs the energetics of two oxygenated species, $ToMOH_{peroxo}$ and $T201_{peroxo}$.[23] Our studies further suggested that the transfer of a proton to either the peroxo unit or an adjacent shifting carboxylate ligand (E231) during dioxygen activation can determine the geometry of oxygenated diiron(III) intermediates as either $ToMOH_{peroxo}$ or $T201_{peroxo}$, respectively (Chart 1B).[21]

Although accurate stopped-flow kinetic parameters for the formation and decay of $ToMOH_{peroxo}$ could not be measured in the T201S variant, time-dependent Mössbauer spectra obtained from freeze-quench investigations of its reaction with O_2 in the presence of ToMOD revealed values comparable to those

Received: March 7, 2011
Revised: April 28, 2011
Published: May 19, 2011

Chart 1. Dioxygen Chemistry in (A) Wild-Type ToMOH and (B) the T201S Variant of ToMOH at 4 °C and pH 7

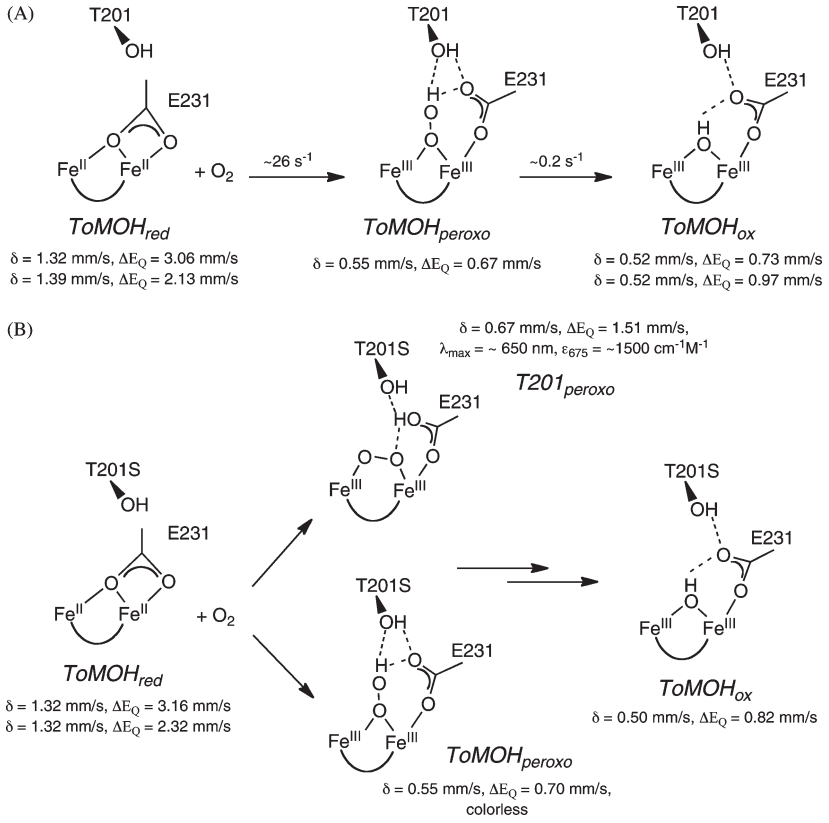

previously obtained with the wild-type enzyme.[20] The data suggested that $T201_{peroxo}$ and $ToMOH_{peroxo}$ are generated by separate pathways,[19,20] with $T201_{peroxo}$ forming more rapidly than $ToMOH_{peroxo}$, their rate constants (k_{form}) being 85 ± 11 and ~26 s^{-1}, respectively, at 4 °C and pH 7.0. Moreover, the decay rate constant of $T201_{peroxo}$ at this temperature (2.9 s^{-1}) is much smaller than k_{form} of $ToMOH_{peroxo}$ (~26 s^{-1}), further consistent with $T201_{peroxo}$ and $ToMOH_{peroxo}$ forming by separate pathways during dioxygen activation.

To further probe the properties of $T201_{peroxo}$ and $ToMOH_{peroxo}$ in T201 variants of ToMOH, we explore in this study three plausible scenarios: (i) that $T201_{peroxo}$ and $ToMOH_{peroxo}$ are formed and react consecutively, (ii) that $T201_{peroxo}$ and $ToMOH_{peroxo}$ form and react independently, and (iii) that $T201_{peroxo}$ and $ToMOH_{peroxo}$ are in equilibrium, with one dominating subsequent reactivity. From the kinetics of the reaction of $T201_{peroxo}$ with arene substrates, followed by monitoring changes in its optical spectrum, we were able to evaluate these three working models for formation and decay of $T201_{peroxo}$ and $ToMOH_{peroxo}$ and to identify the arene-oxidizing intermediate(s). Aromatic hydroxylation by $T201_{peroxo}$ was monitored in the three T201 variants, T201S, T201C, and T201G, previously determined to form the intermediate, although with distinct kinetics. These experiments were conducted with the use of phenol as an external substrate or by converting I100, a residue in the proximity of the active site, into tryptophan as an internal substrate. In addition to the kinetic studies of $T201_{peroxo}$, the amount of the oxidized phenol or I100W was quantitated in the three T201 variants to further explore the role of T201 during catalysis.

EXPERIMENTAL PROCEDURES

General Considerations. Plasmids containing the genes for expressing toluene/*o*-xylene monooxygenase components were supplied by the laboratory of A. Di Donato (Naples, Italy). All ToMO components and ToMOH T201X mutants (X = S, C, or G) were prepared as described previously.[20,24] I100W/T201X double mutants (X = S, C, G, or V) were obtained by using the pET22b(+)/touBEA T201X vector with I100W primers (5′-CAA CTT CAC TTC GGA GCG TGG GCA CTT GAA GAA TAC G-3′ and 5′-C GTA TTC TTC AAG TGC CCA CGC TCC GAA GTG AAG TTG-3′). DNA sequences were confirmed by the MIT-BioPolymers Laboratory. Vectors were transformed into *Escherichia coli* strain BL21(DE3) cells for protein expression. Cell growth and protein purification procedures were the same as for the wild-type enzyme. An iron assay was performed, as described previously.[19,24]

Kinetic Studies of Oxygenated Intermediates in T201X or T201X/I100W (X = S, C, G, or V). UV−vis spectra of $T201_{peroxo}$[20,21] and I100W radical species[25] were monitored as described. Optical bands originating from $T201_{peroxo}$ and the I100W radical were monitored by using a HiTech DX2 stopped-flow spectrophotometer. The drive syringes and flow lines of this instrument were made anaerobic by passage of at least 10 mL of an anaerobic solution of 4 mM sodium dithionite in 25 mM MOPS, pH 7 buffer. The excess dithionite was removed by flushing the syringes with anaerobic buffer. T201X or T201X/I100W ToMOH proteins (~100−200 μM) were reduced anaerobically by reacting the protein with excess sodium dithionite in the presence of an equimolar amount of methyl viologen for

10 min. The reduced protein ($ToMOH_{red}$) was dialyzed against 1 L of 25 mM MOPS, pH 7.0 buffer for ~3 h, anaerobically. Following dialysis, the regulatory protein (ToMOD) was added to the reduced ToMOH. The solution was transferred to a tonometer and loaded into the anaerobic stopped-flow instrument. This solution was rapidly mixed against an equal volume of O_2-saturated 25 mM MOPS, pH 7.0 buffer. The temperature was thermostated at 4 °C using a circulating water bath. Time-dependent optical changes at wavelengths corresponding to the formation and decay of $T201_{peroxo}$ (675 nm) and to the I100W radical species (500 nm) were collected using a PMT (photomultiplier tube) following halogen lamp illumination or a diode array with a xenon lamp. Data were analyzed with Kinetic Studio (TgK Scientific) and Origin 6.1 (OriginLab Corp.) as described previously.[15,20,26] For the T201S and T201G ToMOH variants, an analytical function derived from a $ToMOH_{red} \rightarrow T201_{peroxo} \rightarrow ToMOH_{ox}$ model was applied to obtain formation and decay rate constants for $T201_{peroxo}$. For the T201C variant, an analytical function corresponding to the $ToMOH_{red} \rightarrow T201_{peroxo} \rightarrow T201_{peroxo}^* \rightarrow ToMOH_{ox}$ model was derived to measure the formation and two decay rate constants of $T201_{peroxo}$. In the T201X/I100W variants, the formation and decay of the $T201_{peroxo}$ and I100W radical species were fit to analytical functions derived for $ToMOH_{red} \rightarrow T201_{peroxo} \rightarrow ToMOH_{ox}$ and I100W radical precursor → I100W radical → oxidized product of I100W models, respectively.

Kinetics of an Oxygenated Intermediate in the Reactions with Arene Substrates. The arene substrate phenol was dissolved in dioxygen-saturated buffer, and the solution was rapidly mixed with $ToMOH_{red}D$ in a single-mixing stopped-flow spectrophotometer at 4 °C. Time-dependent optical changes arising from the formation and decay of $T201_{peroxo}$ were then analyzed, as described previously.[21]

For a kinetic isotope effect (KIE) measurement, phenol-2,3,4,5,6-d_5 (hereafter phenol-d_5) (98 at. % D) purchased from Sigma-Aldrich was used without further purification. For kinetic solvent isotope effect (KSIE) measurements, deuterium oxide (99.9 at. % D) purchased from Cambridge Isotope Laboratories or Icon Isotopes was used to prepare 25 mM MOPS, pL 7.0 buffer. The pL value was adjusted by adding an appropriate amount of a NaOD solution (Aldrich). Dioxygen activation of $ToMOH_{red}D$ was monitored at 5 °C, which was thermostated using a circulating water bath.

RESULTS AND DISCUSSION

Decay of $T201_{peroxo}$ in the Presence of Aromatic Substrates. To determine whether $T201_{peroxo}$ is kinetically competent to hydroxylate aromatic substrates, we monitored its formation and decay rates in the presence of phenol. Phenol was selected as a substrate because the natural substrates, toluene and *o*-xylene, are less soluble in water. In addition, ToMO displays a high steady-state activity with phenol.[19] To observe its effects on the decay rate of $T201_{peroxo}$, we dissolved phenol in dioxygen-saturated buffer and rapidly mixed it with the same volume of a solution containing reduced T201X ToMOH and ToMOD. Changes in absorbance at 675 nm, corresponding to formation and decay of $T201_{peroxo}$, were monitored using stopped-flow optical spectroscopy (Figure 1). The rate constants were then obtained by the fit to an analytical function derived from a model involving two or three consecutive, irreversible steps.

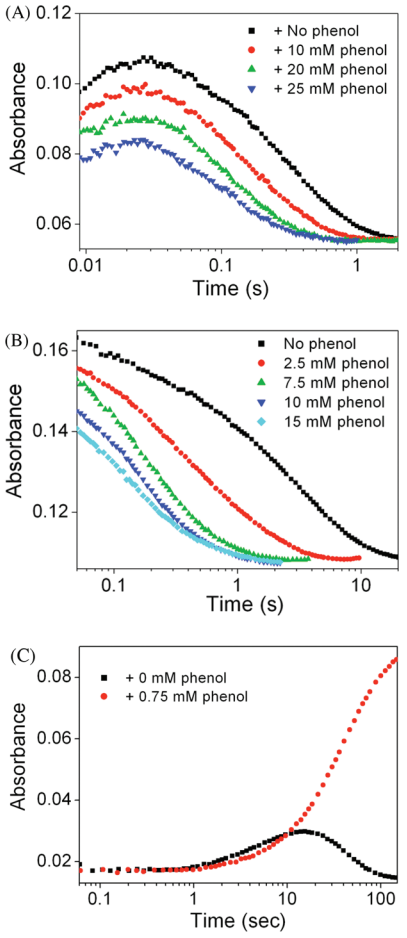

Figure 1. Trace of $T201_{peroxo}$ at 675 nm in the absence and presence of phenol in T201 variants of ToMOH: (A) T201S, (B) T201C, and (C) T201G.

In the reaction of phenol and dioxygen with the T201S variant of $ToMOH_{red}D$, the rate of formation of $T201_{peroxo}$ was within error unaltered over a 0−25 mM range of phenol concentrations (Figure 2A). This result indicates that the substrate does not affect the mechanism of dioxygen activation to form $T201_{peroxo}$. The presence of phenol, however, accelerated the decay of $T201_{peroxo}$, thereby diminishing the accumulation of this intermediate (Figure 1A). Because the rate of decay of $T201_{peroxo}$ in the presence of phenol is much faster than the rate of catechol production measured under steady-state conditions,[20] it is apparent that $T201_{peroxo}$ is kinetically competent for, and probably on the pathway to, phenol oxidation. A plot of k_{decay} versus phenol concentration yielded a linear relationship, from which we could derive a second-order rate constant of 0.18 ± 0.02 s^{-1} mM^{-1} (Figure 2A).

$T201_{peroxo}$ is also observed during dioxygen activation of the T201C and T201G variants of ToMOH. $T201_{peroxo}$ reacts in a similar manner with phenol in the T201C and T201G ToMOH variants. In the absence of arene substrate, $T201_{peroxo}$ in the T201C variant decays by two consecutive processes, $T201_{peroxo} \rightarrow T201_{peroxo}^* \rightarrow ToMOH_{ox}$. Two decay rate constants, k_{decay1} and k_{decay2}, corresponding to the conversion of $T201_{peroxo}$ to $T201_{peroxo}^*$ and of $T201_{peroxo}^*$ to $ToMOH_{ox}$, respectively, were obtained. The change in the absorbance of $T201_{peroxo}$ at 675 nm in the T201C variant was recorded in the absence and presence of

dx.doi.org/10.1021/bi200340f |*Biochemistry* 2011, 50, 5391–5399

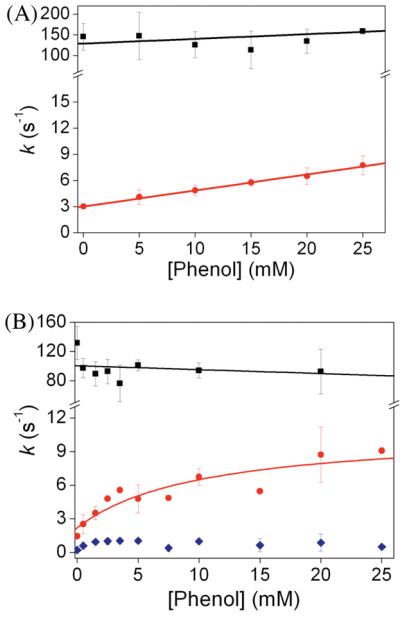

Figure 2. Plots of $T201_{peroxo}$ formation and decay rate constants vs phenol concentration in the reaction of T201X $ToMOH_{red}D$ with phenol in dioxygen-saturated buffer: (A) T201S and (B) T201C. Formation and decay rates are represented with black squares and red circles, respectively. For the T201C variant, second decay rate constants are shown as navy diamonds. Formation and decay rate constants are plotted with either a linear or a saturation function. The results of fits for the formation and decay rates are represented as black and red lines, respectively.

Scheme 1

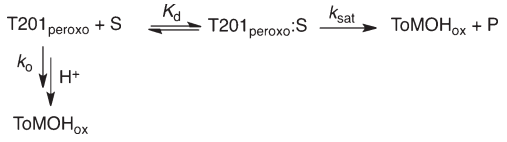

arene substrate (Figure 1B). As described above for the T201S variant, the rate of formation of $T201_{peroxo}$ was within error independent of phenol concentration (Figure 2B). Less $T201_{peroxo}$ accumulated when the concentration of phenol was increased because of the acceleration of its decay rate. A plot of the first derived decay rate constant (k_{decay1}) versus phenol concentration displayed saturation-type behavior (Figure 2B) and was fit (eq 1) to the processes depicted in Scheme 1, resulting in k_{sat} and K_d values of $9 \pm 2\ s^{-1}$ and 10 ± 8 mM, respectively. The second decay process (k_{decay2}) was slightly perturbed by the presence of phenol, but with no clear dependence on its concentration, suggesting that $T201_{peroxo}$* may not react directly with substrate.

$$k_{obs} = k_o + \frac{k_{sat}[S]}{k_d + [S]} \quad (1)$$

To study further the arene-oxidizing mechanism of $T201_{peroxo}$, phenol-d_5 was used in the reaction of T201C $ToMOH_{red}D$ with dioxygen. Arene oxidation typically involves a hybridization change from sp^2 to sp^3 at a phenol carbon atom, and accordingly, an inverse kinetic isotope effect (KIE < 1) was observed.[27] In this manner, the rate of decay of $T201_{peroxo}$ arising from the use of phenol-h_5 versus phenol-d_5 and the resulting KIE can signal kinetic coupling to reaction with phenol. An inverse KIE of 0.82 ± 0.05, listed in Table 1, was derived, indicating that the decay of $T201_{peroxo}$ is kinetically linked to arene oxidation. $T201_{peroxo}$ presumably attacks the arene ring in an electrophilic manner to generate an arene oxide species.[19] No KIE was observed for the following decay step, $T201_{peroxo}$* → $ToMOH_{ox}$. As suggested above, $T201_{peroxo}$* is probably not involved in arene oxidation.

Table 1. Consecutive Decay Kinetic Constants for $T201_{peroxo}$ in the Reaction of T201C $ToMOH_{red}D$ with Phenol in Dioxygen-Saturated Buffer

	phenol-h_5	phenol-d_5	KIE
k_{decay1} (s^{-1})	7.2 ± 0.3	8.7 ± 0.3	0.82 ± 0.05
k_{decay2} (s^{-1})	2.2 ± 0.2	2.1 ± 0.2	1.1 ± 0.1

Table 2. Consecutive Decay Rate Constants and KSIE Values for $T201_{peroxo}$ in the Reaction of T201C $ToMOH_{red}D$ with Dioxygen in H_2O or D_2O Buffer

	H_2O	D_2O	KSIE
k_{decay1} (s^{-1})	1.9 ± 0.1	0.557 ± 0.007	3.4 ± 0.3
k_{decay2} (s^{-1})	0.241 ± 0.004	0.0382 ± 0.0001	6.5 ± 0.1

Reaction of T201G $ToMOH_{red}D$ with a solution of phenol in dioxygen-saturated buffer also led to the formation of $T201_{peroxo}$ (Figure 1C). The kinetic behavior of this reaction could not be monitored, however, because the oxidized product, catechol, binds to the diiron core, forming a Fe(III)-catecholate species with characteristic strong, interfering optical bands between 600 and 1020 nm that mask the optical feature of $T201_{peroxo}$.[28] Binding of catechol to the resting-state enzyme after a single turnover was also observed for the wild type and T201S and T201C variants of ToMOH, but the rates of decay of $T201_{peroxo}$ for the T201S and T201C variants were much faster than the rates of formation of Fe(III)-catecholate species so that optical changes at 675 nm, corresponding to the decay of $T201_{peroxo}$, were not obscured as they were for the T201G variant (data not shown).

Kinetic Solvent Isotope Effect in the Decay of $T201_{peroxo}$ in the Absence and Presence of Arene Substrates. A kinetic solvent isotope effect (KSIE) can be measured when deuterium oxide (D_2O) is used instead of H_2O as the solvent.[29] A proposed chemical mechanism for $T201_{peroxo}$ decay in the absence of arene substrate is protonation of the hydroperoxo unit and subsequent release of hydrogen peroxide.[19,21] If $T201_{peroxo}$ requires a proton(s) in the decomposition pathway and the proton translocation step is coupled to decay of $T201_{peroxo}$, a KSIE of >1 will be observed. The KSIE derived from the rates of decay of $T201_{peroxo}$ in the presence of arene substrate, however, can be altered depending on whether the reaction is linked to arene oxidation, because a typical KIE for aromatic hydroxylation differs from that for proton translocation, as described above. We therefore derived KSIE values from the rates of decay of $T201_{peroxo}$ in the absence and presence of phenol to distinguish the kinetically prevailing chemical step in $T201_{peroxo}$ decay and to provide an additional assessment of our previous conclusion that the more enhanced decay of $T201_{peroxo}$ upon addition of phenol is an indication of its kinetic competence.

To measure the KSIE for the decay of $T201_{peroxo}$, we monitored the reaction of T201C $ToMOH_{red}D$ with dioxygen

dx.doi.org/10.1021/bi200340f |*Biochemistry* 2011, 50, 5391–5399

Table 3. Consecutive Decay Rate Constants and KSIE Values for $T201_{peroxo}$ in the Reaction of T201C $ToMOH_{red}D$ with Dioxygen and 10 mM Phenol in H_2O or D_2O Buffer

	H_2O	D_2O	KSIE
k_{decay1} (s^{-1})	7.2 ± 0.3	6.26 ± 0.07	1.15 ± 0.06
k_{decay2} (s^{-1})	2.2 ± 0.2	1.02 ± 0.03	2.1 ± 0.2

in H_2O or D_2O buffer at 5 °C. Two consecutive rates of decay of $T201_{peroxo}$ were observed in D_2O buffer, as previously seen in H_2O buffer. The k_{decay1} and k_{decay2} values measured in the two buffers returned a $KSIE_{decay1}$ of 3.4 ± 0.3 and a $KSIE_{decay2}$ of 6.5 ± 0.1 (Table 2). These large KSIE values for the decay process can imply multiple protons in a decay pathway,[30] which presumably, for $T201_{peroxo}$, involve protonation of the peroxo moiety and release of H_2O_2. $KSIE_{decay}$ values of >1 were observed for the T201S and T201G variants, 1.40 ± 0.11 and 10.6 ± 1.6, respectively (data not shown). $KSIE_{decay}$ values obtained from the rates of decay of $T201_{peroxo}$ increase in the order T201S < T201C < T201G, possibly because of their increasingly poor ability to facilitate proton transfer during the decomposition of $T201_{peroxo}$.

Different $KSIE_{decay}$ results were obtained when experiments were conducted in the presence of phenol. KSIE studies in the presence of phenol were conducted with only T201C but not the T201S and T201G variants. Although the $KSIE_{decay}$ in T201S > 1, it is not large enough to permit an accurate value to be obtained in the presence of phenol. For the T201G variant, formation of the optical bands of Fe(III)-catecholate, as described previously, made it impossible to measure the $KSIE_{decay}$. A solution of T201C $ToMOH_{red}D$ in either H_2O or D_2O buffer was therefore mixed with dioxygen-saturated buffer containing 10 mM phenol. Rates of decay of $T201_{peroxo}$ in each buffer were measured, yielding $KSIE_{decay}$ values of 1.15 ± 0.06 and 2.1 ± 0.2 for two successive steps, respectively (Table 3). The dramatically reduced KSIE value for the first decay step compared to that determined in the absence of phenol, 3.4 ± 0.3, indicates that decay of $T201_{peroxo}$ is no longer entirely dependent on solvent protons but primarily involves an interaction of the peroxodiiron(III) intermediate with phenol. Therefore, the significant decrease in KSIE values due to introduction of the arene substrate supports the conclusion that $T201_{peroxo}$ is kinetically competent to hydroxylate phenol. The $KSIE_{decay}$ result for the second decay process (k_{decay2}) is also considerably perturbed by addition of phenol. Because $T201_{peroxo}$* probably does not react with phenol, as discussed above, the presence of phenol must trigger as yet unidentified reactions, for example, conformational changes that contribute to the decay of $T201_{peroxo}$*.

Studies of T201X/I100W Variants (X = S, C, G, or V). As reported previously, I100 is located near the diiron active site where it helps to form a hydrophobic pocket.[18] When I100 was mutated to W, the indole ring of the installed tryptophan approached the iron atoms, with Fe···C distances ranging from 6.0 to 11.9 Å.[31] Addition of dioxygen to the reduced form of I100W ToMOH and ToMOD demonstrated that the variant activates O_2 at a rate similar to that observed for the wild-type enzyme. The rate of decay of $ToMOH_{peroxo}$ was accelerated, however, because the tryptophan residue serves as a substrate closely positioned near the active site, reacting with $ToMOH_{peroxo}$ to form diiron(III,IV) and I100W radical species.[31] The generation of the I100W radical from $ToMOH_{peroxo}$ was nearly quantitative, and time-dependent RFQ/Mössbauer, EPR, and UV−vis spectroscopic studies revealed that the $ToMOH_{peroxo}$ decay rate corresponds to the rate of formation of the I100W radical species.

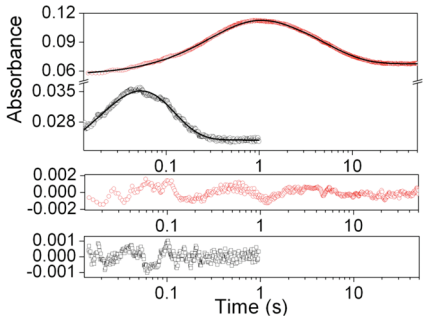

Figure 3. Time-dependent optical changes in the reaction of T201S/I100W $ToMOH_{red}D$ with dioxygen at 675 nm (black squares) and 500 nm (red circles) fit to a function representing two consecutive, irreversible processes. Fitting results are represented as black lines in spectra and with residuals shown below.

On the basis of these findings, T201X/I100W double mutants were prepared to examine the effect of the tryptophan residue on the rate of decay of $T201_{peroxo}$ as well as the rate of formation of the anticipated I100W radical. I100W/T201X variants of ToMOH, prepared as described previously (X = S, C, G, or V), all contained ∼4 iron atoms/protein. When reduced T201S/I100W ToMOH and ToMOD were mixed with dioxygen-saturated buffer in the stopped-flow spectrophotometer at 4 °C, changes in the optical spectra at 675 and 500 nm originating from $T201_{peroxo}$ and I100W radical species, respectively, were observed (Figure 3 and Figure S1 of the Supporting Information). From the data, we computed rates of formation and decay of $T201_{peroxo}$ and the I100W radical species by fitting the optical changes to a function representing two consecutive, irreversible processes (Table 4). The rates of both formation and decay of $T201_{peroxo}$ and I100W radical species in T201S/I100W were greatly perturbed compared to their values in T201S or I100W single variants.[32] An accelerated rate of decay of $T201_{peroxo}$ in T201S/I100W, compared to that in the T201S variant, implies that $T201_{peroxo}$ is on the reaction pathway of I100W oxidation, as discussed above for phenol oxidation. Three mechanisms were proposed to account for these data, as portrayed in Scheme 2. The increased $T201_{peroxo}$ decay rate rules out mechanism A in Scheme 2, whereby $T201_{peroxo}$ irreversibly decomposes to $ToMOH_{peroxo}$. If mechanism A were operative, only the decay rate of $ToMOH_{peroxo}$, but not that of $T201_{peroxo}$, would be accelerated by introduction of the arene substrate, tryptophan.

Both formation and decay of the I100W radical species are well fit by a single-exponential function (Figure 3 and Table 4), which indicates that there is only one kinetically observable precursor, either $T201_{peroxo}$ or $ToMOH_{peroxo}$, but not both. These data therefore exclude mechanism B in Scheme 2. The decay rate constant for $T201_{peroxo}$, 14.9 ± 0.4 s^{-1}, however, is much larger than the formation rate constant of the I100W radical species, 2.8 ± 0.1 s^{-1}, indicating that $T201_{peroxo}$ does not directly convert to the I100W radical species. These results indicate that an additional species, presumably $ToMOH_{peroxo}$, exists along the decay reaction pathway.

A third possible mechanism that we considered is one in which $T201_{peroxo}$ and $ToMOH_{peroxo}$ are in equilibrium with one

Table 4. Rates of Formation and Decay of $T201_{peroxo}$ and W Radical Intermediates Generated During Dioxygen Activation of I100W, T201S, and T201S/I100W $ToMOH_{red}D$

	I100W	T201S	T201S/I100W
$T201_{peroxo}$	nd[a]	$k_{form} = 88 \pm 7\ s^{-1}$, $k_{decay} = 3.1 \pm 0.3\ s^{-1}$	$k_{form} = 55 \pm 14\ s^{-1}$, $k_{decay} = 14.9 \pm 0.4\ s^{-1}$
I100W radical	$k_{form} = 0.804 \pm 0.001\ s^{-1}$,[b] $k_{decay} = 0.054 \pm 0.002\ s^{-1}$	nd[a]	$k_{form} = 2.88 \pm 0.12\ s^{-1}$, $k_{decay} = 0.19 \pm 0.01\ s^{-1}$

[a] Not determined. [b] Taken from ref 31.

Scheme 2. Reaction Models for the Formation and Decay of $T201_{peroxo}$ during Dioxygen Activation of T201X/I100W ToMOH[a]

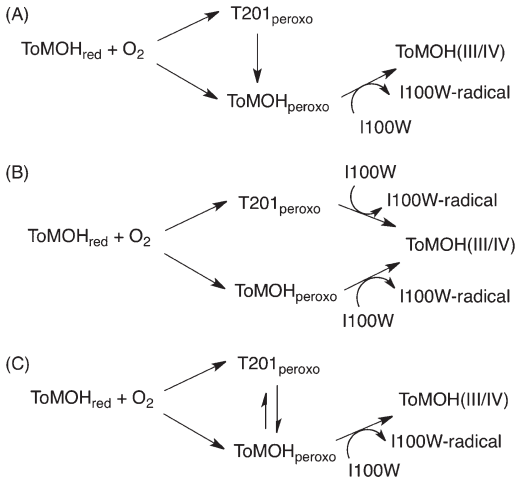

[a] $ToMOH_{red}$ and ToMOH(III/IV) represent diiron(II/II) and diiron(III/IV) redox states, respectively.

another (mechanism C in Scheme 2). This possibility is supported by the observed kinetic properties of the $T201_{peroxo}$ and I100W radical intermediates in the T201S, I100W, and T201S/I100W variants. The chemical equilibrium conveys kinetic competence to $T201_{peroxo}$ in arene oxidation, although this intermediate does not directly react with the substrate. Depletion of $ToMOH_{peroxo}$ by reaction with I100W converts $T201_{peroxo}$ to $ToMOH_{peroxo}$ to maintain the equilibrium.

A possible mechanism for the interconversion of $ToMOH_{peroxo}$ and $T201_{peroxo}$ is suggested in Scheme 3. A hydrogen-bonded proton on the hydroperoxo unit of $ToMOH_{peroxo}$ or on an oxygen atom of the adjacent glutamate (E231) in $T201_{peroxo}$ can easily shift between the two positions, as illustrated in the scheme. Such proton translocation can trigger reorganization of the peroxo unit, altering the geometry of oxygenated diiron(III) species. The relative energetics of the two geometries, 1,1-peroxodiiron(III) and 1,2-peroxodiiron(III), computed by QM/MM methods,[23] suggest the energy difference between $ToMOH_{peroxo}$ and $T201_{peroxo}$ to be relatively small, and the occurrence of both intermediate species is therefore energetically plausible.

Introduction of I100W has a similar effect on the kinetic properties of $T201_{peroxo}$ in the other T201 variants. For T201C/I100W, formation of $T201_{peroxo}$ and the I100W radical species were monitored during the reaction of T201C/I100W $ToMOH_{red}D$ with O_2, as described for the T201S/I100W variant. Formation and decay of $T201_{peroxo}$ and the I100W radical species in T201C/I100W monitored at 675 and 500 nm, respectively (Figure S2 of

Scheme 3. Proposed Mechanism for the Interconversion of $T201_{peroxo}$ and $ToMOH_{peroxo}$

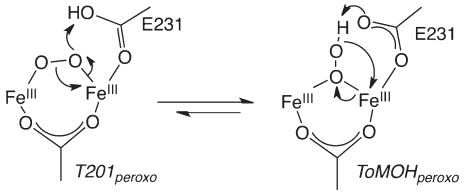

the Supporting Information), and time-dependent traces were fit to a consecutive two-exponential function without inclusion of $T201_{peroxo}$* in the decomposition pathway of $T201_{peroxo}$ to $ToMOH_{ox}$ (Table S1 of the Supporting Information). Given that a consecutive three-exponential function was required to fit the trace of $T201_{peroxo}$ in the T201C single variant, the rapid decay of $T201_{peroxo}$ in the reaction with the I100W residue does not proceed through $T201_{peroxo}$*. Acceleration of the rate of decay of $T201_{peroxo}$ in T201C/I100W relative to the value in the T201C variant (k_{decay1}) again supports a mechanism in which $T201_{peroxo}$ is on the pathway of aromatic hydroxylation through equilibrium with $ToMOH_{peroxo}$ (Scheme 2C).

Rates of both formation and decay of the I100W radical species in T201C/I100W are accelerated by comparison to those of I100W and T201S/I100W variants (Table S1 of the Supporting Information). These kinetic characteristics of the I100W radical species in T201C/I100W can be perturbed if the local environment near the active sites is significantly altered. Previous studies with the I100W variant of ToMOH revealed that the rates of formation and decay of I100W radical species are pH-dependent.[31] The rates are accelerated at high pH values, suggesting that deprotonation at the tryptophan residue during formation and decay of I100W radical species is preceded by a fast oxidation. Therefore, the acceleration of the rates of formation and decay of I100W radical species in T201C/I100W relative to rates in the I100W or T201S/I100W variant possibly reflects local pH changes near the active site, induced by the T201C mutation. Because T201C is a poorer residue than T201 or T201S for facilitating H_3O^+ transport to the diiron center, the T201C variant may experience an increase in local pH at the active site.

The T201G/I100W variant also generated the I100W radical species during dioxygen activation (Table S1 and Figure S2 of the Supporting Information). No $T201_{peroxo}$ species could be observed, however, probably because it reacts rapidly with I100W and does not accumulate to a detectable level.

Finally, dioxygen activation by the T201V/I100W variant was investigated (Table S1 and Figure S2 of the Supporting Information). As expected from the T201V single-variant study,[21] $T201_{peroxo}$ was not detected in T201V/I100W. Possibly proton translocation, required to generate $T201_{peroxo}$, is too slow;

Table 5. Quantification of I100W Radical Species Generated in T201X/I100W ToMOH

	I100W	T201S/ I100W	T201C/ I100W	T201G/ I100W	T201V/ I100W
coupling (%)	55 ± 1	49 ± 1	36 ± 2	38 ± 1	31 ± 2

alternatively, formation of the I100W radical is too rapid to allow the intermediate to build up. Another possibility is that the T201V variant energetically disfavors formation of $T201_{peroxo}$.[21,23] Reaction of T201V/I100W $ToMOH_{red}D$ with dioxygen also generated the I100W radical species, possibly because the spectroscopically silent species, $ToMOH_{peroxo}$, formed and reacted with the tryptophan residue. The kinetic properties of the I100W radical species in T201V/I100W are slightly different from those of I100W but rather similar to those of T201C/I100W, indicating that the local pH at the active site might similarly be perturbed because of the presence of the hydrophobic valine side chain.

Quantification of I100W Radical Species in T201X/I100W Double Variants. The wild-type ToMOH displays half-sites reactivity, in which only one of the two diiron centers in the dimeric hydroxylase undergoes productive reactivity during single-turnover experiments. The other site can be reduced to the diiron(II) state but does not simultaneously form $ToMOH_{peroxo}$ upon introduction of O_2.[19] Half-sites reactivity is also consistently observed in reactions with phenol, whereby 50% catechol per diiron sites form during single-turnover experiments.[20,33] In T201S, ~50% phenol oxidation was similarly measured during a single turnover, indicating that the serine variant retains half-sites reactivity.[20] This property seems to be conserved in other T201 variants. Reactions of T201G $ToMOH_{red}D$ with dioxygen generated oxygenated intermediates at approximately half of the diiron centers. If half-sites reactivity is operative in all the T201G, -C, and -V variants, approximately half of the enzyme present in solution would be able to oxidize phenol in single-turnover experiments, but the yields were consistently lower than that value.[21] This result contrasts with our findings for the wild type and T201S variant. These findings indicate that decay of peroxodiiron(III) species is not tightly coupled to oxidation of hydrocarbon substrate when a hydroxyl group is lacking at position 201, presumably leading to release of hydrogen peroxide, rather than catechol, as an uncoupling product.[34]

Single-turnover yields from the reaction of the internal I100W substrate were also determined for T201X/I100W double variants. The extinction coefficient of the I100W radical species at 500 nm is ε_{500} = ~1500 cm^{-1} M^{-1}, based on Mössbauer and stopped-flow UV−vis data.[31] Using this value, we were able to quantitate the amount of I100W radical species generated in reactions of reduced T201X/I100W ToMOH and ToMOD with dioxygen. The amount of I100W radical species produced was measured by taking into account the individual formation and decay rate constants corresponding to the time-dependent spectral changes at 500 nm, as described previously (Table 5).[21] In I100W and T201S/I100W variants, ~50% of the I100W radical species formed per diiron site, which is consistent with half-sites reactivity and ~50% of single-turnover yields during phenol oxidation.[20] By contrast, ~30% of I100W radical species per diiron site were generated in the T201C, -G, and -V variants, even though ~50% of the diiron sites presumably reacted with dioxygen. The uncoupling chemistry in T201C, -G, and -V variants is consistent with the single-turnover yields of these species during phenol oxidation. In addition, the results agree with the steady-state kinetics showing ~70−150-fold lower k_{cat}/K_M values for the T201C, -G, and -V variants compared to the wild-type and T201S enzymes. These results further support the notion that the hydroxyl group at position 201 is necessary for efficient hydrocarbon oxidation.[35]

Comparisons of Oxygenated Intermediates and Their Reactivities in ToMOH and sMMOH. Reaction of sMMOH with dioxygen consecutively generates three oxygenated intermediates, P*, P or H_{peroxo}, and Q, and the latter two species are capable of oxidizing hydrocarbon substrates.[26,36−38] H_{peroxo} and Q react with substrates through different mechanisms, with H_{peroxo} preferring more electron-rich substrates, such as propylene, ethyl vinyl ether, and diethyl ether, and operating by a two-electron transfer process. In contrast, Q favors one-electron transfer chemistry for methane oxidation.[39] The promiscuous reactivity of sMMOH, therefore, can be attributed, at least in part, to the divergent reactions catalyzed by the two distinctive intermediates.

In contrast, ToMOH has evolved specifically to perform aromatic hydroxylation. A wide and long hydrophobic channel, ~6−10 Å × ~30−35 Å, is present only in toluene monooxygenases, where it most likely serves as the pathway for arene substrate access/product egress.[18,40] This structural feature may explain how ToMOH developed specificity for aromatic substrates. To perform aromatic hydroxylation, a high-valent oxygenated species like Q is unnecessary, because one-electron oxidation or C−H homolysis for arenes is not thermodynamically favorable because of their high redox potentials and large C−H bond dissociation energies.[41] An alternative mechanism is most likely operative in ToMOH. Oxidation of the arene can occur via the transfer of two electrons from substrates to an electrophilic oxidant, such as H_{peroxo} in sMMOH, the analogous species proposed for amine oxygenase,[42,43] and a hydroperoxoiron(III) intermediate in cytochrome P450 monooxygenase.[41] The $ToMOH_{peroxo}$ intermediate in ToMOH therefore most likely shares the electronic and geometric structures of hydroperoxoiron(III) or peroxodiiron(III) species rather than those of Q in sMMOH.

A mechanism for the oxidation of arenes by $ToMOH_{peroxo}$ is proposed in Scheme 4. As previously reported,[19] a Hammett plot for the oxidation of *para*-substituted phenols in ToMOH has a negative slope, consistent with the electrophilic character of $ToMOH_{peroxo}$. Electrophilic attack of the hydroperoxo unit in $ToMOH_{peroxo}$ on the arene ring can initiate the oxidation, followed by formation of an arene oxide species, weakly bound to the diiron center. Addition of water and rearrangement can provide the arene product and return the resting-state diiron site. A similar reaction with an arene substrate might be possible for $T201_{peroxo}$, although not kinetically feasible because of the fast conversion to $ToMOH_{peroxo}$. Without such conversion, $T201_{peroxo}$ might participate in futile side reactions, becoming protonated with subsequent O−O bond cleavage and formation of a Q-type product with undesired reactivity.

■ CONCLUDING REMARKS

These kinetic studies of $T201_{peroxo}$ in the absence and presence of external (phenol) or internal (tryptophan, as I100W) substrates clearly demonstrate that $T201_{peroxo}$ is kinetically on the reaction pathway of arene oxidation. Kinetic solvent isotope effects in the reaction of $T201_{peroxo}$ with phenol confirm this kinetic competence. Three reaction models were considered

Scheme 4. Proposed Mechanism of Aromatic Hydroxylation by $ToMOH_{peroxo}$ and $T201_{peroxo}$ in T201 Variants of ToMOH

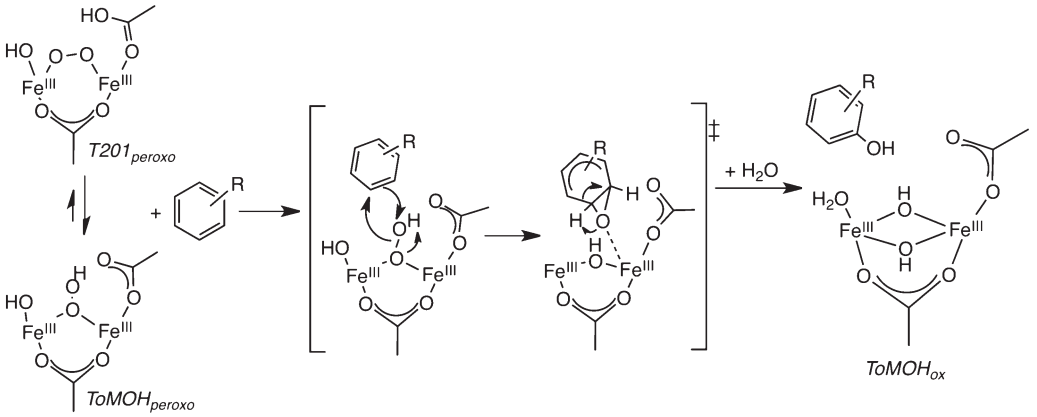

to account for the measured kinetics of $T201_{peroxo}$ and I100W radical species formation and substrate reactivity. The only one that accounts for all of the experimental results requires that $T201_{peroxo}$ be in equilibrium with $ToMOH_{peroxo}$. Acceleration of the rate of decay of $T201_{peroxo}$ in the presence of arene substrates is therefore ascribed to the rapid conversion of $T201_{peroxo}$ to $ToMOH_{peroxo}$, the latter being the reactive species in arene oxidation.

■ ASSOCIATED CONTENT

Ⓢ Supporting Information. Table S1 and Figures S1 and S2. This material is available free of charge via the Internet at http://pubs.acs.org.

■ AUTHOR INFORMATION

Corresponding Author

*E-mail: lippard@mit.edu. Telephone: (617) 253-1892. Fax: (617) 258-8150.

Funding Sources

This work was funded by Grant GM032134 from the National Institute of General Medical Sciences.

■ ACKNOWLEDGMENT

We thank Dr. C. E. Tinberg for helpful comments on the manuscript.

■ ABBREVIATIONS

BMMs, bacterial multicomponent monooxygenases; DFT, density functional theory; EPR, electron paramagnetic resonance; k_{decay}, decay rate constant; k_{form}, formation rate constant; KIE, kinetic isotope effect; KSIE, kinetic solvent isotope effect; sMMOB, regulatory protein of soluble methane monooxygenase; sMMOH, hydroxylase component of soluble methane monooxygenase; MOPS, 3-(*N*-morpholino)propanesulfonic acid; P or H_{peroxo}, second peroxodiiron intermediate of sMMOH; P*, first peroxodiiron intermediate of sMMOH; Q, di(μ-oxo)diiron(IV) intermediate of sMMOH; QM/MM, quantum mechanics/molecular mechanics; RFQ, rapid freeze quench; $T201_{peroxo}$, peroxodiiron(III) intermediates observed in T201 variants; $T201_{peroxo}$*, intermediate generated in the decomposition pathway of $T201_{peroxo}$; ToMO, toluene/*o*-xylene monooxygenase; ToMOD, regulatory protein of ToMO; ToMOH, hydroxylase component of ToMO; $ToMOH_{ox}$, resting state of ToMOH; $ToMOH_{red}$, reduced ToMOH; $ToMOH_{red}$D, reduced ToMOH in complex with ToMOD; $ToMOH_{peroxo}$, diiron(III) intermediate observed in the wild-type ToMOH enzyme.

■ REFERENCES

(1) Merkx, M., Kopp, D. A., Sazinsky, M. H., Blazyk, J. L., Müller, J., and Lippard, S. J. (2001) Dioxygen Activation and Methane Hydroxylation by Soluble Methane Monooxygenase: A Tale of Two Irons and Three Proteins. *Angew. Chem., Int. Ed. 40*, 2782–2807.

(2) Wallar, B. J., and Lipscomb, J. D. (1996) Dioxygen Activation by Enzymes Containing Binuclear Non-Heme Iron Clusters. *Chem. Rev. 96*, 2625–2657.

(3) Solomon, E. I., Brunold, T. C., Davis, M. I., Kemsley, J. N., Lee, S.-K., Lehnert, N., Neese, F., Skulan, A. J., Yang, Y.-S., and Zhou, J. (2000) Geometric and Electronic Structure/Function Correlations in Non-Heme Iron Enzymes. *Chem. Rev. 100*, 235–349.

(4) Nordlund, P., and Eklund, H. (1993) Structure and Function of the *Escherichia coli* Ribonucleotide Reductase Protein R2. *J. Mol. Biol. 232*, 123–164.

(5) Fox, B. G., Shanklin, J., Somerville, C., and Münck, E. (1993) Stearoyl-Acyl Carrier Protein Δ^9 Desaturase from *Ricinus communis* Is a Diiron-Oxo Protein. *Proc. Natl. Acad. Sci. U.S.A. 90*, 2486–2490.

(6) Xing, G., Hoffart, L. M., Diao, Y., Sandeep Prabhu, K., Arner, R. J., Reddy, C. C., Krebs, C., and Bollinger, J. M., Jr. (2006) A Coupled Dinuclear Iron Cluster that Is Perturbed by Substrate Binding in *myo*-Inositol Oxygenase. *Biochemistry 45*, 5393–5401.

(7) Vu, V. V., Emerson, J. P., Martinho, M., Kim, Y. S., Münck, E., Park, M. H., and Que, L., Jr. (2009) Human Deoxyhypusine Hydroxylase, an Enzyme Involved in Regulating Cell Growth, Activates O_2 with a Nonheme Diiron Center. *Proc. Natl. Acad. Sci. U.S.A. 106*, 14814–14819.

(8) Choi, Y. S., Zhang, H., Brunzelle, J. S., Nair, S. K., and Zhao, H. (2008) *In Vitro* Reconstitution and Crystal Structure of *p*-Aminobenzoate *N*-Oxygenase (AurF) Involved in Aureothin Biosynthesis. *Proc. Natl. Acad. Sci. U.S.A. 105*, 6858–6863.

(9) Behan, K. R., and Lippard, S. J. (2010) The Aging-Associated Enzyme CLK-1 Is a Member of the Carboxylate-Bridged Diiron Family of Proteins. *Biochemistry 49*, 9679–9681.

(10) Lee, S.-K., Fox, B. G., Froland, W. A., Lipscomb, J. D., and Münck, E. (1993) A Transient Intermediate of the Methane Monooxygenase Catalytic Cycle Containing an $Fe^{IV}Fe^{IV}$ Cluster. *J. Am. Chem. Soc. 115*, 6450–6451.

(11) Liu, K. E., Wang, D., Huynh, B. H., Edmondson, D. E., Salifoglou, A., and Lippard, S. J. (1994) Spectroscopic Detection of Intermediates in the Reaction of Dioxygen with Reduced Methane Monooxygenase Hydroxylase from *Methylococcus capsulatus* (Bath). *J. Am. Chem. Soc. 116*, 7465–7466.

(12) Liu, K. E., Valentine, A. M., Wang, D., Huynh, B. H., Edmondson, D. E., Salifoglou, A., and Lippard, S. J. (1995) Kinetic and Spectroscopic Characterization of Intermediates and Component Interactions in Reactions of Methane Monooxygenase from *Methylococcus capsulatus* (Bath). *J. Am. Chem. Soc. 117*, 10174–10185.

(13) Lee, S.-K., and Lipscomb, J. D. (1999) Oxygen Activation Catalyzed by Methane Monooxygenase Hydroxylase Component: Proton Delivery during the O−O Bond Cleavage Steps. *Biochemistry 38*, 4423–4432.

(14) Shu, L., Nesheim, J. C., Kauffmann, K., Münck, E., Lipscomb, J. D., and Que, L., Jr. (1997) An $Fe_2^{IV}O_2$ Diamond Core Structure for the Key Intermediate Q of Methane Monooxygenase. *Science 275*, 515–518.

(15) Tinberg, C. E., and Lippard, S. J. (2009) Revisiting the Mechanism of Dioxygen Activation in Soluble Methane Monooxygenase from *M. capsulatus* (Bath): Evidence for a Multi-Step, Proton-Dependent Reaction Pathway. *Biochemistry 48*, 12145–12158.

(16) Notomista, E., Lahm, A., Di Donato, A., and Tramontano, A. (2003) Evolution of Bacterial and Archaeal Multicomponent Monooxygenases. *J. Mol. Evol. 56*, 435–445.

(17) Leahy, J. G., Batchelor, P. J., and Morcomb, S. M. (2003) Evolution of the Soluble Diiron Monooxygenases. *FEMS Microbiol. Rev. 27*, 449–479.

(18) Sazinsky, M. H., Bard, J., Di Donato, A., and Lippard, S. J. (2004) Crystal Structure of the Toluene/*o*-Xylene Monooxygenase Hydroxylase from *Pseudomonas stutzeri* OX1. *J. Biol. Chem. 279*, 30600–30610.

(19) Murray, L. J., Naik, S. G., Ortillo, D. O., García-Serres, R., Lee, J. K., Huynh, B. H., and Lippard, S. J. (2007) Characterization of the Arene-Oxidizing Intermediate in ToMOH as a Diiron(III) Species. *J. Am. Chem. Soc. 129*, 14500–14510.

(20) Song, W. J., Behan, R. K., Naik, S. G., Huynh, B. H., and Lippard, S. J. (2009) Characterization of a Peroxodiiron(III) Intermediate in the T201S Variant of Toluene/*o*-Xylene Monooxygenase Hydroxylase from *Pseudomonas* sp. OX1. *J. Am. Chem. Soc. 131*, 6074–6075.

(21) Song, W. J., McCormick, M. S., Behan, R. K., Sazinsky, M. H., Jiang, W., Jeffery, L., Krebs, C., and Lippard, S. J. (2010) Active Site Threonine Facilitates Proton Transfer during Dioxygen Activation at the Diiron Center of Toluene/*o*-Xylene Monooxygenase Hydroxylase. *J. Am. Chem. Soc. 132*, 13582–13585.

(22) Song, W. J., Gucinski, G., Sazinsky, M. H., and Lippard, S. J. (2011) manuscript submitted for publication.

(23) Bochevarov, A. D., Li, J., Song, W. J., Lippard, S. J., and Friesner, R. A. (2011) Insights into Different O_2-Chemistry of Methane and Toluene Monooxygenase Hydroxylases. *J. Am. Chem. Soc. 133*, 7384–7397.

(24) Cafaro, V., Scognamiglio, R., Viggiani, A., Izzo, V., Passaro, I., Notomista, E., Dal Piaz, F., Amoresano, A., Casbarra, A., Pucci, P., and Di Donato, A. (2002) Expression and Purification of the Recombinant Subunits of Toluene/*o*-Xylene Monooxygenase and Reconstitution of the Active Complex. *Eur. J. Biochem. 269*, 5689–5699.

(25) Murray, L. J., García-Serres, R., Naik, S., Huynh, B. H., and Lippard, S. J. (2006) Dioxygen Activation at Non-Heme Diiron Centers: Characterization of Intermediates in a Mutant Form of Toluene/*o*-Xylene Monooxygenase Hydroxylase. *J. Am. Chem. Soc. 128*, 7458–7459.

(26) Beauvais, L. G., and Lippard, S. J. (2005) Reactions of the Peroxo Intermediate of Soluble Methane Monooxygenase Hydroxylase with Ethers. *J. Am. Chem. Soc. 127*, 7370–7378.

(27) Mitchell, K. H., Rogge, C. E., Gierahn, T., and Fox, B. G. (2003) Insight into the Mechanism of Aromatic Hydroxylation by Toluene 4-Monooxygenase by Use of Specifically Deuterated Toluene and *p*-Xylene. *Proc. Natl. Acad. Sci. U.S.A. 100*, 3784–3789.

(28) Cox, D. D., and Que, L., Jr. (1988) Functional Models for Catechol 1,2-Dioxygenase. The Role of the Iron(III) Center. *J. Am. Chem. Soc. 110*, 8085–8092.

(29) Quinn, D. M., and Sutton, L. D. (1991) Theoretical Basis and Mechanistic Utility of Solvent Isotope Effects. In *Enzyme Mechanism from Isotope Effects*, CRC Press, Boca Raton, FL.

(30) Vidakovic, M., Sligar, S. G., Li, H., and Poulos, T. L. (1998) Understanding the Role of the Essential Asp251 in Cytochrome P450cam Using Site-Directed Mutagenesis, Crystallography, and Kinetic Solvent Isotope Effect. *Biochemistry 37*, 9211–9219.

(31) Murray, L. J., García-Serres, R., McCormick, M. S., Davydov, R., Naik, S. G., Kim, S.-H., Hoffman, B. M., Huynh, B. H., and Lippard, S. J. (2007) Dioxygen Activation at Non-Heme Diiron Centers: Oxidation of a Proximal Residue in the I100W Variant of Toluene/*o*-Xylene Monooxygenase Hydroxylase. *Biochemistry 46*, 14795–14809.

(32) Dramatic changes due to the I100W residue in $T201_{peroxo}$ formation rate constants will be described separately.

(33) Tinberg, C. E., Song, W. J., Izzo, V., and Lippard, S. J. (2011) Multiple Roles of Component Proteins in Bacterial Multicomponent Monooxygenases: Phenol Hydroxylase and Toluene/*o*-Xylene Monooxygenase from *Pseudomonas* sp. OX1. *Biochemistry 50*, 1788–1798.

(34) We attempted to quantitate the concentration of H_2O_2 in this reaction, but the catalase activity of ToMO led to an inaccurate measurement of H_2O_2 produced during single-turnover experiments.

(35) Elsen, N. L., Bailey, L. J., Hauser, A. D., and Fox, B. G. (2009) Role for Threonine 201 in the Catalytic Cycle of the Soluble Diiron Hydroxylase Toluene 4-Monooxygenase. *Biochemistry 48*, 3838–3846.

(36) Valentine, A. M., Stahl, S. S., and Lippard, S. J. (1999) Mechanistic Studies of the Reaction of Reduced Methane Monooxygenase Hydroxylase with Dioxygen and Substrates. *J. Am. Chem. Soc. 121*, 3876–3887.

(37) Brazeau, B. J., and Lipscomb, J. D. (2000) Kinetics and Activation Thermodynamics of Methane Monooxygenase Compound Q Formation and Reaction with Substrates. *Biochemistry 39*, 13503–13515.

(38) Tinberg, C. E., and Lippard, S. J. (2010) Oxidation Reactions Performed by Soluble Methane Monooxygenase Hydroxylase Intermediates H_{peroxo} and Q Proceed by Distinct Mechanisms. *Biochemistry 49*, 7902–7912.

(39) Baik, M.-H., Gherman, B. F., Friesner, R. A., and Lippard, S. J. (2002) Hydroxylation of Methane by Non-Heme Diiron Enzymes: Molecular Orbital Analysis of C−H Bond Activation by Reactive Intermediate Q. *J. Am. Chem. Soc. 124*, 14608–14615.

(40) Bailey, L. J., McCoy, J. G., Phillips, G. N., Jr., and Fox, B. G. (2008) Structural Consequences of Effector Protein Complex Formation in a Diiron Hydroxylase. *Proc. Natl. Acad. Sci. U.S.A. 105*, 19194–19198.

(41) Meunier, B., de Visser, S. P., and Shaik, S. (2004) Mechanism of Oxidation Reactions Catalyzed by Cytochrome P450 Enzymes. *Chem. Rev. 104*, 3947–3980.

(42) Korboukh, V. K., Li, N., Barr, E. W., Bollinger, J. M., Jr., and Krebs, C. (2009) A Long-Lived, Substrate-Hydroxylating Peroxodiiron(III/III) Intermediate in the Amine Oxygenase, AurF, from *Streptomyces thioluteus*. *J. Am. Chem. Soc. 131*, 13608–13609.

(43) Li, N., Korboukh, V. K., Krebs, C., and Bollinger, J. M., Jr. (2010) Four-Electron Oxidation of *p*-Hydroxylaminobenzoate to *p*-Nitrobenzoate by a Peroxodiferric Complex in AurF from *Streptomyces thioluteus*. *Proc. Natl. Acad. Sci. U.S.A. 107*, 15722–15727.